Air Quality, Atmosphere & Health (2021) 14:1313–1323
https://doi.org/10.1007/s11869-021-01023-9

Impact of emissions from a single urban source on air quality estimated from mobile observation and WRF-STILT model simulations

Hao Fan[1] · Chuanfeng Zhao[1] · Yikun Yang[1] · Xingchuan Yang[1] · Chunying Wang[2]

Received: 22 December 2020 / Accepted: 31 March 2021 / Published online: 16 April 2021

Abstract

For industrial cities, quantifying the influence of a given emission source on air quality is very important for making a detailed control strategy to the emissions. By taking use of the mobile observations and WRF-STILT model simulations, this study analyzes the air pollution characteristics and air quality influences from an industrial emission source in Xinji, China. During the study period, the hourly average concentrations of smoke, SO_2, and NO_x emitted from the industrial source are 1.01, 22.04, and 26.22 mg/m^3, respectively. The mobile observations show that with the increase of distance from the emission source, the concentration of air pollutants increases first and then decreases. The peak values of $PM_{2.5}$, SO_2, and NO_x appear at the distance of around 0–3 km away from the emission source, among which $PM_{2.5}$ and SO_2 increase first and then decrease before stabilizing, while NO_x is interfered by emissions from the traffic along the roads. Within the distance of 3 km, the emission source has obvious influence on the air quality with contribution rate 10–48% at night time and 3–23% at day time. The simulation results of WRF-STILT also support the observed gradient change characteristics of air pollutants, suggesting that this industrial emission source is an important pollution source for regions around it. Our results further show that the meteorological conditions play an important role on the transport capacity of industrial emissions. The results of this study provide support for quantifying the scope of influence of fixed emission sources, especially in industrial cities.

Keywords Mobile observation · $PM_{2.5}$ · Air quality · WRF-STILT · Emission contribution

Introduction

With the accelerated urbanization and industrial over-development, air pollution has been an urgent environment problem worldwide. Air pollution can not only cause negative effects on human health but also exacerbate extreme weather events (Cohen et al. 2017; Li et al. 2016; Li et al. 2020; Zhang et al. 2019; Zhao et al. 2018; Zhao et al. 2020). Since 2013, the frequent occurrence of fine particulate matter with aerodynamic diameters less than 2.5 μm (i.e., $PM_{2.5}$) pollution exceedances in many areas of China has drawn the concerns of the government and the public (An et al. 2019; Sahu et al. 2020; Zhao et al. 2019). During recent years, particularly since 2013 when air pollution control measures were taken in China, the concentration of air pollutants has obviously decreased (Fan et al. 2020a; Li et al. 2019; Zhang et al. 2019). However, the spatial distribution of air pollutants is uneven, especially in the Beijing-Tianjin-Hebei region, with high concentration of air pollutants at some local regions (Chen et al. 2019; Dang and Liao 2019; Kontkanen et al. 2020; Li et al. 2020; Shi et al. 2018). At present, China's air pollution control urgently needs to analyze the impact of emissions at different spatial scales (Li et al. 2019; Vandyck et al. 2018).

Existing studies have indicated that the major factors to determine air pollution include emission, meteorological conditions, transport, and atmospheric chemistry (An et al. 2019; Fan et al. 2020a; Huang et al. 2019; Yang et al. 2016; Zhao et al. 2019). Currently, emission is still the main cause of air pollution in China. So, it is still valuable and necessary to carry out a series of studies

✉ Chuanfeng Zhao
czhao@bnu.edu.cn

[1] State Key Laboratory of Earth Surface Processes and Resource Ecology, and College of Global Change and Earth System Science, Beijing Normal University, Beijing 100875, China

[2] Hebei Sailhero Environmental Protection Hi-tech., Ltd, Shijiazhuang 050035, Hebei, China

on the impact of emission sources on air quality. The sources of air pollution include natural, domestic, industrial, and traffic emission sources (Doherty et al. 2017; Zhai et al. 2018). Previous studies focused more on the spatial distribution of pollution sources and the analysis of monitoring results at fixed locations (Heintzenberg et al. 2020; Wang et al. 2019). However, there are few studies regarding the influence on air quality by emissions from a single source, particularly in China. Considering that the information about the impacts of single emission source is essential to making accurate and detailed air quality control strategies, this study aims to investigate the potential impacts on air quality by a single emission source using both mobile observation and model simulation analysis.

Mobile observation is a powerful means to quantitatively understand the characteristics of regional air pollution, which will further provide a basis for air quality controls. Compared with the observations at fixed ground stations, mobile observation has the wide monitoring range and strong maneuverability (Fischer et al. 2015; Li et al. 2018). And compared with remote sensing observations, it has higher time resolution and can carry out real-time measurements (Hilario et al. 2020; Mao et al. 2020). Therefore, mobile observation is an effective technical means for tracking the diffusion and emission source of air pollutants. It is helpful to deepen the understanding to regional air pollution distribution characteristics and conveying laws.

The model simulation is another important way for investigating the air pollution diffusion (Georgiou et al. 2018; Hu et al. 2017). The Weather Research and Forecast (WRF) coupled with the Stochastic Time-Inverted Lagrangian Transport (STILT) model (WRF-STILT) can effectively provide both forward and backward trajectories from the simulation (Lin et al. 2003; Zhao et al. 2009). By combining the WRF-STILT simulations and observations on regional meteorological characteristics, we can easily identify the transport and contribution of air pollutants from a typical emission source to air quality at surrounding regions. Actually, the WRF-STILT model has been widely used in atmospheric environment researches (Brophy et al. 2019; Fan et al. 2020b; Hu et al. 2018; Jeong et al. 2012a, 2012b; Zhao et al. 2009).

In this study, we carry out a systematical analysis on the spatial distribution and characteristics of pollutants from a typical industrial pollution source in Xinji, an industrial city in the Beijing-Tianjin-Hebei (BTH) region, by using both mobile observations and model simulations. The paper is organized as follows. "Data and method" describes the data and method. "Results and discussion" analyzes the mobile observation results of air pollutants and the results of the WRF-STILT model simulations in Xinji, Hebei Province. "Conclusions" summarizes the findings.

Data and method

Study area

Xinji is an industrial city in Hebei Province, and it is also one of the cities which lie in the transport channel of air pollutants in the BTH region (Chen et al. 2019). As shown in Fig. 1, it is about 240 km, 220 km, and 65 km away from three major cities of Beijing, Tianjin, and Shijiazhuang in BTH region, respectively. Therefore, the emission of air pollutants in Xinji has large potential impacts on the air quality of the whole BTH region. We selected a major factory in Xinji to conduct a comprehensive study on the transport and influence of air pollutants emitted from it. The factory releases the air pollutants with a chimney at height 53 m, which has an inner diameter of 1.9 m. The schematic diagram of the study area and the periphery of the factory are shown in Fig. 1. Note that the factory name is not provided in this study for confidential consideration.

Observation

The real-time online emission data is used to examine the emission characteristics. The data include total exhaust emission, smoke, SO_2, and NO_x mass concentration with hourly time resolution. Specifically, the smoke sampling is obtained by extractive condensation, and the total exhaust emission is calculated by measuring the flow rate and cross-sectional area. The mobile observations are used to obtain the concentration of air pollutants around the factory. In this study, the concentrations of $PM_{2.5}$, SO_2, and NO_2 are used in the analysis. The monitoring equipment installed in the mobile vehicle is XHAQMS4000 mobile air quality monitoring system (http://www.sailhero.com/product/131.html). It consists of four modules, namely, SO_2 and CO monitoring module, NO_x and O_3 monitoring module, particulate matter ($PM_{2.5}$ and PM_{10}) monitoring module, and man-machine interaction and communication module. The data acquisition standard and quality control standard are based on the ambient air quality standards (GB 3095-2012). Table S1 shows the main indicators of air pollutant monitoring instruments. In addition, the sampling inlet is located on the right side of the top of the vehicle, and the vehicle exhaust port is located on the lower left of the vehicle. This design is to avoid the influence of the vehicle's own exhaust gas on the measurement results.

As shown in Table 1, the mobile observation was carried out four times on September 19 to 21, 2019, with different winds and weather types. Note that the times used in this study are all local time. Starting from the location where factory's exhaust chimney lies in, the mobile observation was made within the distance range of about 0–7 km. Two time periods of 13:00–16:00 and 21:00–24:00 are adopted simply because the atmospheric mixed boundary layer (MBL) height varies

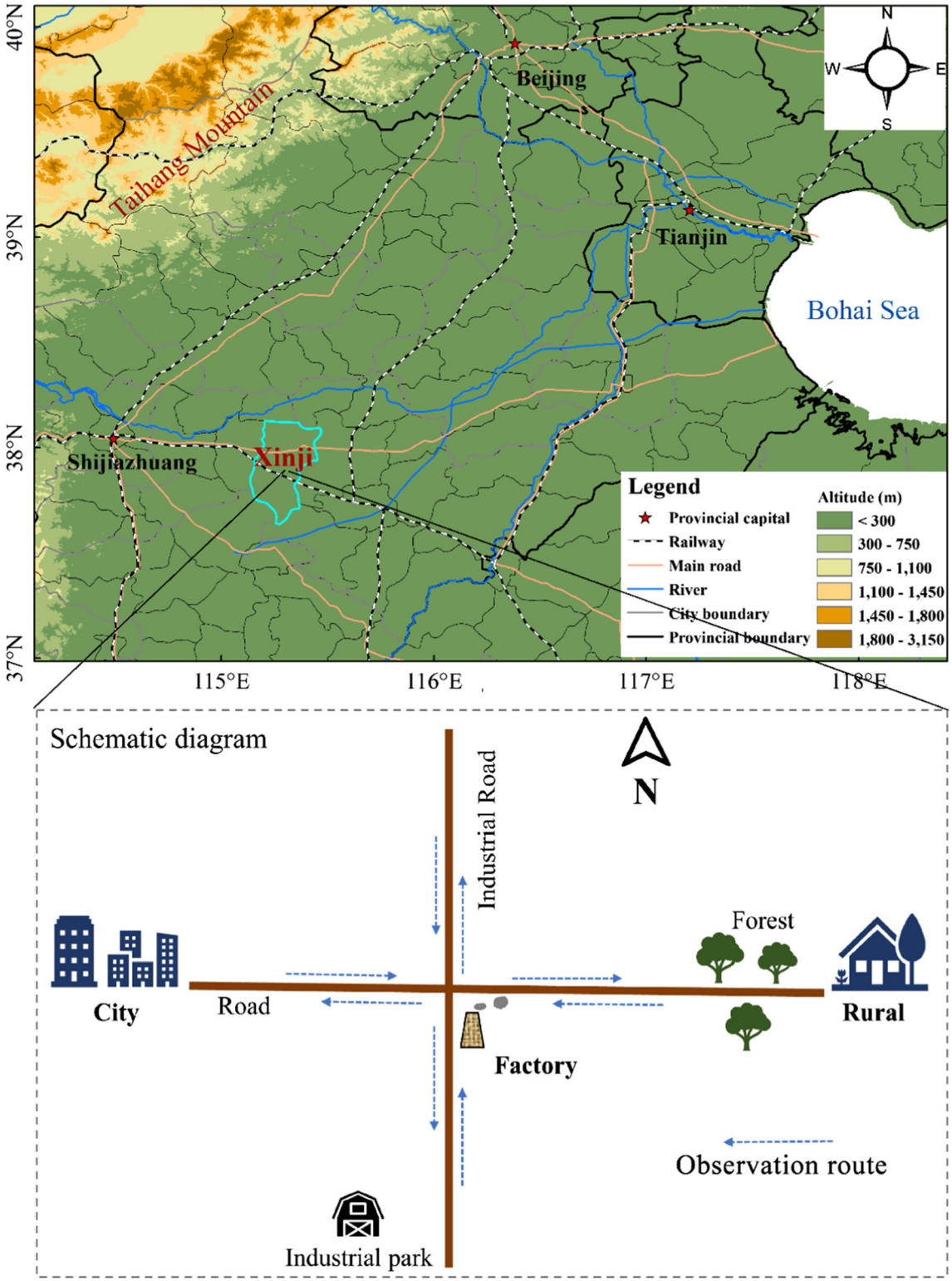

Fig. 1 The schematic diagram of the study area. The above figure shows the location of Xinji, and the following figure shows the factory and its surroundings. To be confidential, the factory name is not provided in this study

little (at least weakly) during these two periods, which can help us to limit the air pollution changes caused by MBL variations. During the mobile observation period, the weather was mainly cloudy and sunny, and the wind speed was basically lower than 11 km/h, which was suitable for observation (Table 1). The direction that the mobile observation goes

Table 1 Overview of mobile observation time and direction, along with the winds and weather type during the mobile observation time

Date	Time	Driving direction	Wind direction	Wind speed	Weather type
2019.9.19	21:00–24:00	North and east	Southwest	10.6 km/h	Cloudy
2019.9.20	13:00–16:00	East and south	North	<1 km/h	Cloudy
2019.9.21	13:00–16:00	East and west	West	4.4 km/h	Sunny
2019.9.21	21:00–24:00	East and west	East	9.3 km/h	Sunny

towards roughly follows the direction of the smoke plume at the observation time. We mainly carry out tracking observations in the downwind direction, and make round-trip observations in each direction and then take use of their average values. In order to ensure the reliability of sampling data, our vehicle speed was controlled within 20 km/h. It should be noted that due to the road restrictions and other factors during the implementation, the actual mobile observation paths are slightly adjusted. The monitoring module of SO_2 failed on September 21, 2019, so the SO_2 on that day was not analyzed in the subsequent analysis.

WRF-STILT model simulation

In this study, we use the WRF-STILT model to simulate the forward trajectories, and obtain the footprint distribution map. The WRF-STILT model is widely used for the study of the transport of atmospheric gases, including both polluted gases and greenhouse gases (Fan et al. 2020b; Zhao et al. 2009; Zhao et al. 2019). The details of the WRF-STILT model have been described in previous studies (Jeong et al. 2012a, 2012b; Lin et al. 2003; Nehrkorn et al. 2010). Here, we only introduce the settings relevant to this study.

The initial and boundary meteorological conditions for the WRF setup are based on the National Centre for Environmental Prediction final reanalysis data. The simulation domain is 100 km × 100 km, with a horizontal resolution of 0.5 km. The main physical module settings of WRF operation are the same as that used in our previous studies (Fan et al. 2020b; Zhao et al. 2009; Zhao et al. 2019) and are not repeated here. For the STILT setup, 1000 particles are released hourly at the chimney location (53 m) and transported forward in time duration of 1 h.

The analysis method for contribution rate

Based on the $PM_{2.5}$ concentration obtained by the mobile observation, we calculate the contribution rate from the emission source to the ambient air pollution. The method used here follows that proposed by Zhao et al. (2019). The contribution rate is calculated using the following equation:

$$CR_{i,\ d} = \frac{PM_{2.5i,d} - PM_{2.5\mathrm{min}d}}{PM_{2.5i,d}}$$

where i is the observation direction and d is the observation distance (0–7 km). CR is the contribution rate and $PM_{2.5min}$ is the minimum $PM_{2.5}$ mass concentration. This method has been proved effective for the calculation of local emission contribution based on the ground observation data (Zhao et al. 2019). In particular, we choose the lowest value of $PM_{2.5}$ in each route as the background value, and the difference between the observed concentration values at different distances and the background value is then treated as the contribution from the factory emissions. By doing this, we have assumed that there are no extra point or line emission sources within the study region, which is roughly reasonable considering the dominant emission of the factory within the study domain in our case. However, the vehicle emissions along the roads and other small emission sources in the region do introduce potential uncertainties to our analysis, which is beyond the capability of current study and could be investigated further in the future.

Results and discussion

Characteristics of online emission

Figure 2 shows the hourly variations of total exhaust emissions, smoke, SO_2, and NO_x from the factory examined during the study period. The total exhaust emissions range from 60,000 to 95,000 m^3/h, with a great variation range. We found that 11:00–19:00 and around 24:00 every day are the two time periods with high values of total emissions (Fig. 2a). In contrast, the changes of smoke emission are relatively weak with values between 0.9 and 1.1 mg/m^3 (Fig. 2b). During the study period, the smoke emission drops obviously at 20:00 on September 21, which is consistent with the sudden drop time of total exhaust emissions. There are many sources of primary aerosols, but emissions from industrial activities in many regions are considered as an important source of $PM_{2.5}$ (Ohara et al. 2007; Zhao et al. 2019). In particular, the proportion of inhalable particulates in smoke is high. Therefore, emission of smoke can obviously increase the proportion of particulate matter in the surrounding atmosphere, especially for the primary particulate matter emitted (Huang et al. 2019; Zhao et al. 2019).

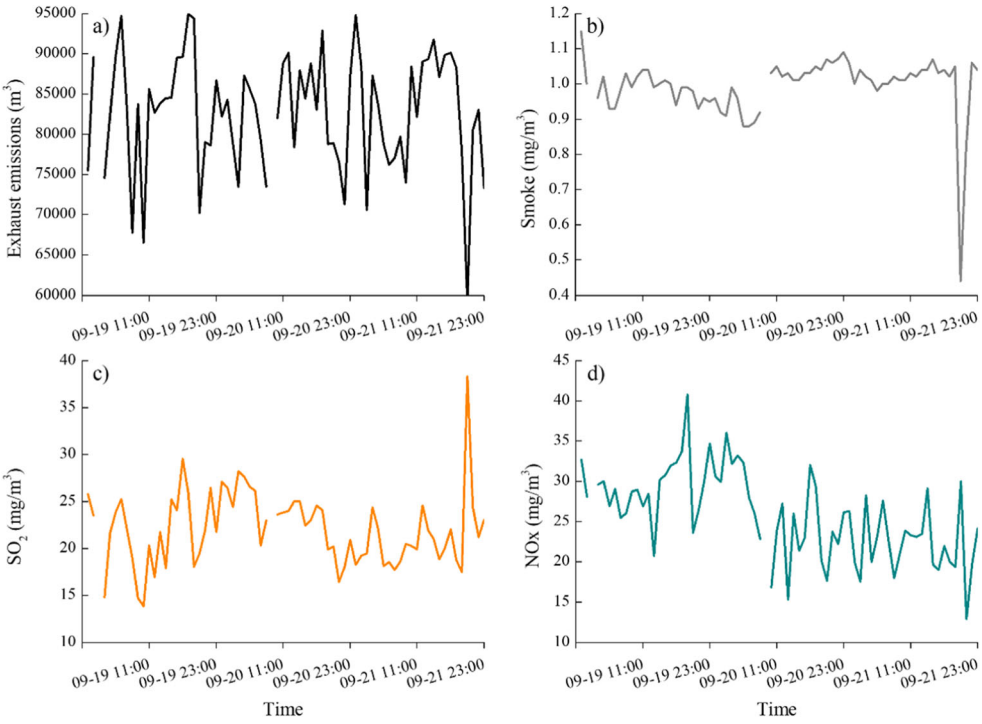

Fig. 2 The hourly variation of real-time online emission of total exhaust pollutants, smoke, SO_2, and NO_x from the factory examined

The concentration of sulfur oxides and nitrogen oxides in the nearby atmosphere depends on the emission of SO_2 and NO_x to a certain extent (Feng et al. 2020; Kuik et al. 2018). According to the results shown in Fig. 2c, the changes of SO_2 emission were not obvious while with a high value appeared on September 21. The average NO_x emissions from September 19 to 21 were 29.41, 25.92, and 22.26 mg/m^3 in sequence, showing a clear decreasing trend. The results shown in Fig. 2 about the real-time emission from the factory examined suggest that the factory is a large emission enterprise source in Xinji, and has provided relatively stable (with certain variations) emissions during our observation period. Actually, the factory is the absolutely major source of local air pollutants in the study area.

Mobile observation analysis

Around the target factory, we carried out mobile observations for 3 days in 4 different periods, as shown in Table 1. Corresponding to the online emission data, we mainly analyze the concentrations of $PM_{2.5}$, SO_2, and NO_2. On September 19, we carried out the first mobile observation from 21:00 to 24:00, and the results are shown in Fig. 3. The observations from the factory to the east show consistent spatial variations among the concentrations of $PM_{2.5}$, SO_2, and NO_2. With the increase of distance away for the factory, the concentrations of $PM_{2.5}$, SO_2, and NO_2 increase first and then decrease. The concentrations of $PM_{2.5}$, SO_2, and NO_2 reach the peaks at a distance near 500 m, 1500 m and 3000 m, respectively, and then have an obvious decreasing trend afterward before reaching the location that they weakly fluctuate around a relatively low value (setting as background value in this study). The distance from the factory to the location that the air pollutant becomes relatively stable with a low value can be defined as the influential distance of the factory emissions. These spatial variation characteristics of air pollutants are most likely related to their physical and chemical properties. Compared with sulfide and nitrogen oxides, the sedimentation rate of particulate matter is faster (Lachatre et al. 2019). Therefore, the peak value of $PM_{2.5}$ concentration appears at a distance closer to the factory, and the influential distance of the factory emissions for $PM_{2.5}$ is smaller (shorter in distance) than that for SO_2 and NO_2 (Fig. 3 e and f).

We found that when going to the north, the mobile observation results show the similar trends (Fig. 3 b, d, and f). First, $PM_{2.5}$ has an obvious upward trend with distance before reaching the peak value at about 1500 m, and then has a declining trend before stabilizing around a relatively low value. This spatial variation has a strong relationship with the meteorological conditions at that time, especially the wind direction and speed. The stronger conveying capacity to the north led to the peak position of $PM_{2.5}$ being farther than that to the east. This is also confirmed by the WRF-STILT simulation results that will be shown in Fig. 6. The concentrations of SO_2 and NO_2 have peak values at distances 1000 m and 500 m, respectively. Differently, the concentrations of SO_2 and NO_2 increase again after the distance of 4000 m and 5000 m, respectively. Further analysis found that there are some small factories located on both sides of the road at 4 km away from the factory examined in the direction towards

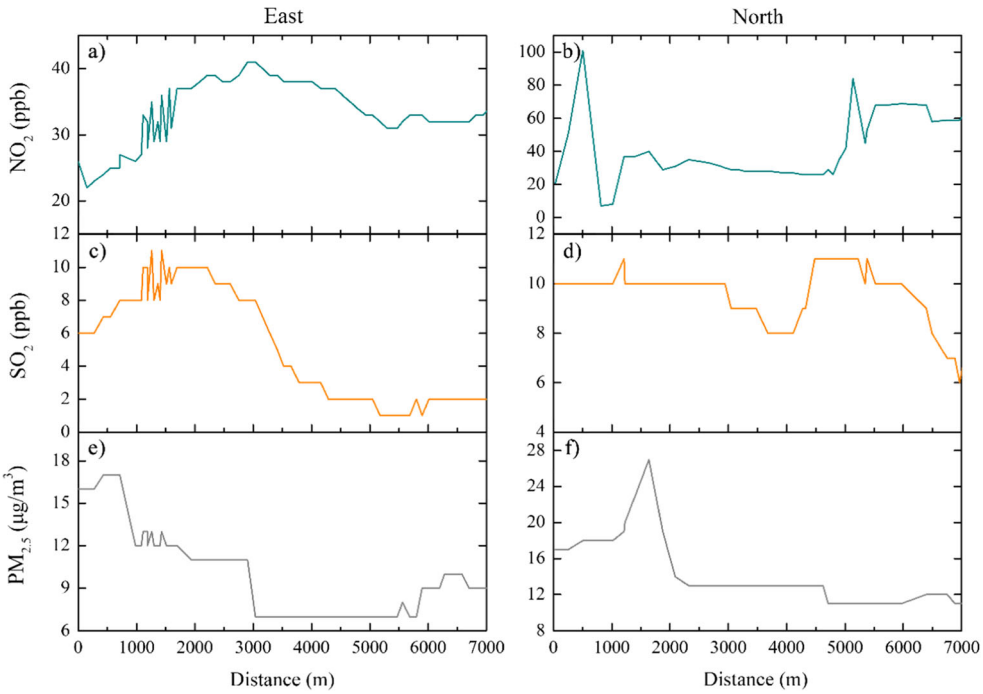

Fig. 3 The spatial variations of $PM_{2.5}$, SO_2, and NO_2 along the mobile observation paths from the factory location to the east or north during the period from 21:00 to 24:00 on September 19, 2019

the north. Although the emissions of these enterprises are much lower than those from the target factory, they inevitably affect the concentrations of SO_2 and NO_2 in the north direction, particularly when the mobile vehicle is closer to them.

On the afternoon of September 20, the mobile observations were carried out in the directions towards the east and south, as shown in Fig. 4. We found that the concentration changes of $PM_{2.5}$ and SO_2 can obviously show the gradient changes (increase first and then decrease) with spatial distance. The observation results of SO_2 and $PM_{2.5}$ in the eastward direction show that the concentrations have the high values within 3 km, decrease after 3 km, and finally get stabilized around a low value. Noting that the road towards the east is a road having access to the countryside (Fig. 1), the observations along this road are less affected by other potential emission sources. As for NO_2, it shows large fluctuations in the south direction with values about 2–4 times of that observed in the east

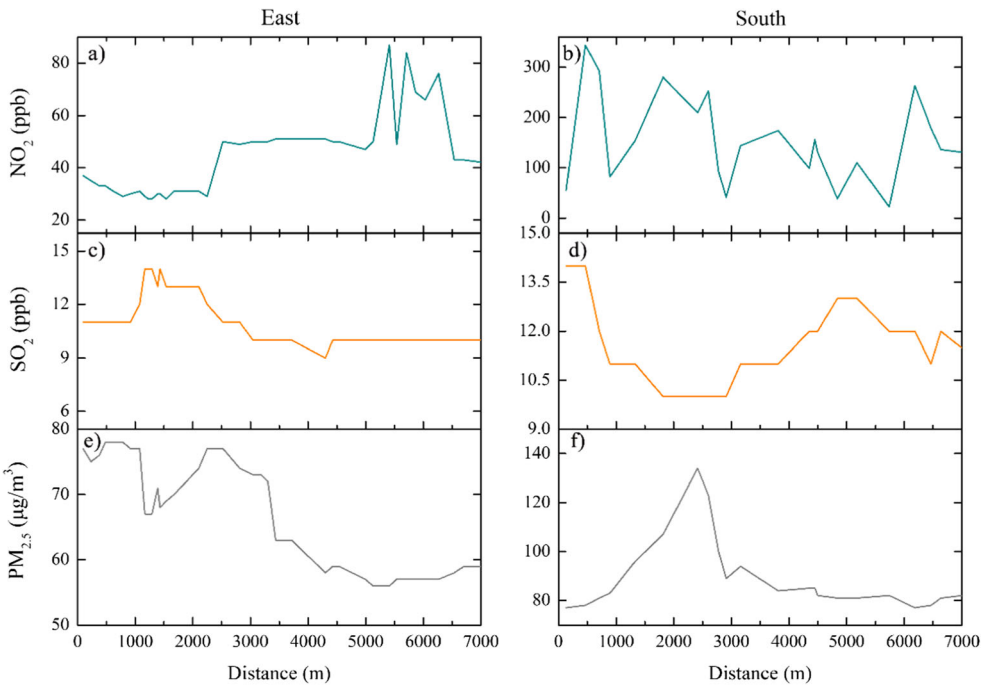

Fig. 4 The spatial variations of $PM_{2.5}$, SO_2, and NO_2 along the mobile observation paths from the factory location to the east or north during the period from 13:00 to 16:00 on September 20, 2019

direction, suggesting the most likely contributions from vehicles on the road. The other two observations in the afternoon and evening on September 21 also show the similar patterns as shown in Figs. 3 and 4, which are shown in Figs. S1–S2. For example, on the evening of September 21, the peak values of NO_2 lie at the distances of 1.5 km towards the west direction and 2.5 km towards the east direction, and the peak values of $PM_{2.5}$ lie at the distances of 750 m and 1500 m in the west and east directions, respectively.

According to the results of four mobile observations, the concentration fluctuation of NO_2 is relatively larger and the absolute value of NO_2 concentration is larger along the south-north direction than that along the east direction. Previous studies show that traffic emission is one of the main sources of NO_2 pollution in cities (Cheng et al. 2020; Ding et al. 2017; Lugon et al. 2020). The road in the north-south direction has much more traffic flow than the road in the east direction, making the NO_2 concentration much more affected by the traffic emission. Another feature obtained from the four mobile observations is that the NO_2 and $PM_{2.5}$ concentrations have more fluctuations (variations) in the daytime than that at nighttime, which might be also related to the influence of traffic. There are more vehicles on the road at daytime, and the exhaust emission and dust have a certain impact on the observation results (Cheng et al. 2020; Dang and Liao 2019). In addition, human production activities and photochemical processes are more frequent during the daytime than at night, which could also have a contribution (An et al. 2019; Fan et al. 2020a). As indicated earlier, the in-depth analysis about the impacts from these potential sources other than the factory is beyond this study and could be done in the future.

As our observation results show, there are relatively large spatial variations in NO_2 and SO_2. In city, the main anthropogenic sources of NO_2 are motor vehicle emissions and industrial emissions, while SO_2 is more from fossil fuel combustion (Ding et al. 2017; Feng et al. 2020). Previous studies have found that NO_2 can generate NO under the action of solar radiation, and in turn, NO and ozone can be converted into NO_2 (Cheng et al. 2020; Li et al. 2019). NO_2 and NO are the main nitrogen-containing pollutants in the atmosphere, which together form NO_x. As for SO_2, its lifetime in the atmosphere is relatively short, and it also has a relatively active chemical conversion process (Lachatre et al. 2019). Combined with the results of existing studies and our observations, the emissions and atmospheric chemistry both affect the final observation results of NO_2 and SO_2. Although it is difficult to describe the entire process of air pollutant emissions and changes in atmospheric composition in our current research, gaseous pollutants seem to be more sensitive to other factors besides primary emissions.

Contribution rate analysis

Based on the analysis results from mobile observations as shown in section 3.2, we choose $PM_{2.5}$ as the representative variable to investigate the contribution rate of factory's emissions to the air pollutant concentration of surrounding regions. As indicated in the method section, we choose the lowest value of $PM_{2.5}$ in each route of mobile observations as the background value, and the difference between the observed $PM_{2.5}$ concentration and the background value is calculated. The ratio of this difference to the observed $PM_{2.5}$ concentration is then considered as the contribution rate of the factory emissions (Zhao et al. 2019). According to the gradient change of mobile observations as shown in Figs. 3–4 and Figs. S1–S2, we calculated the emission impact within 3 km from the factory. Regions with distances farther than 3 km is not studied because with the distance farther away from the factory, the relative contribution from other potential emission sources close to the vehicle becomes important, making the calculation more uncertain.

Figure 5 shows the average contribution rate calculated in each direction. Obviously, the factory has a strong influence on the air pollution around it, and the contribution ratio at night is obviously higher than that during the daytime. At night, the contribution rate within 3 km is 10–48%, with an average of about 32%. In contrast, the contribution rate during the daytime is about 3–23%. On the one hand, the photochemical reaction at night is much weaker than that during the daytime, and the traffic emissions and other anthropogenic activities are also relatively less (Cheng et al. 2020; Dang and Liao 2019), which highlight the significant contribution from the factory examined. On the other hand, the field records during the study period show that at night, the wind speed is slightly faster than that during the day, it accelerates the diffusion speed of pollutants and expands the influence

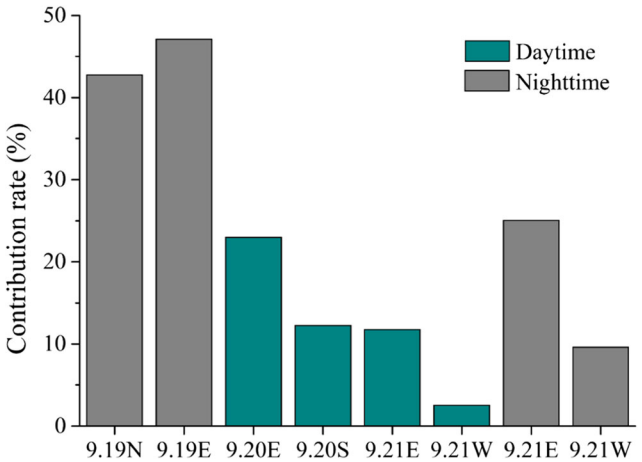

Fig. 5 Contribution rate of the target factory emission source to ambient air pollutants. N, S, W, and E indicate north, south, west, and east, respectively

area of pollution (Fan et al. 2020b; Huang et al. 2019). Although there are other factors inevitably affecting the concentration of $PM_{2.5}$, all of our observations during the experiments confirm that the factory's emission has a great influence on the surrounding air quality.

WRF-STILT simulation results

We use the WRF-STILT model to simulate the forward trajectories, which is carried out in the same period as the observations (Fig. 6). The model simulations show basically the same consistent results with our mobile observations: more pollutant particles are found for locations closer to the factory. Note that the simulation results are more driven by meteorological variables (Fan et al. 2020b; Zhao et al. 2009). The simulation results show that on September 19, the particles are mainly diffused to the north, and in the next 2 days, the particles are mainly diffused to the west. This result suggests that the driving directions for our mobile observations are reliable, which are actually determined based on the plume direction (Table 1). In addition, the simulation results in Fig. 6 show that the pollutants spread farther away at night than in daytime, which is consistent with the information obtained from field observations (Fig. S3).

Figure 6 shows that although the diffusion area of pollutants increases with the increase of distance from the target point, the particle concentration decreases rapidly with the increase of distance. This phenomenon is consistent with the finding from previous researches (Fan et al. 2020b; Jeong et al. 2012a; Zhao et al. 2009), which suggests that the air pollution caused by the emission sources at a fixed point has a limited influence range. Therefore, the key for the control of air pollution is to accurately judge the direction and influential distance of pollutants from emission sources, and establish the relationship between emissions from a given source and near surface air

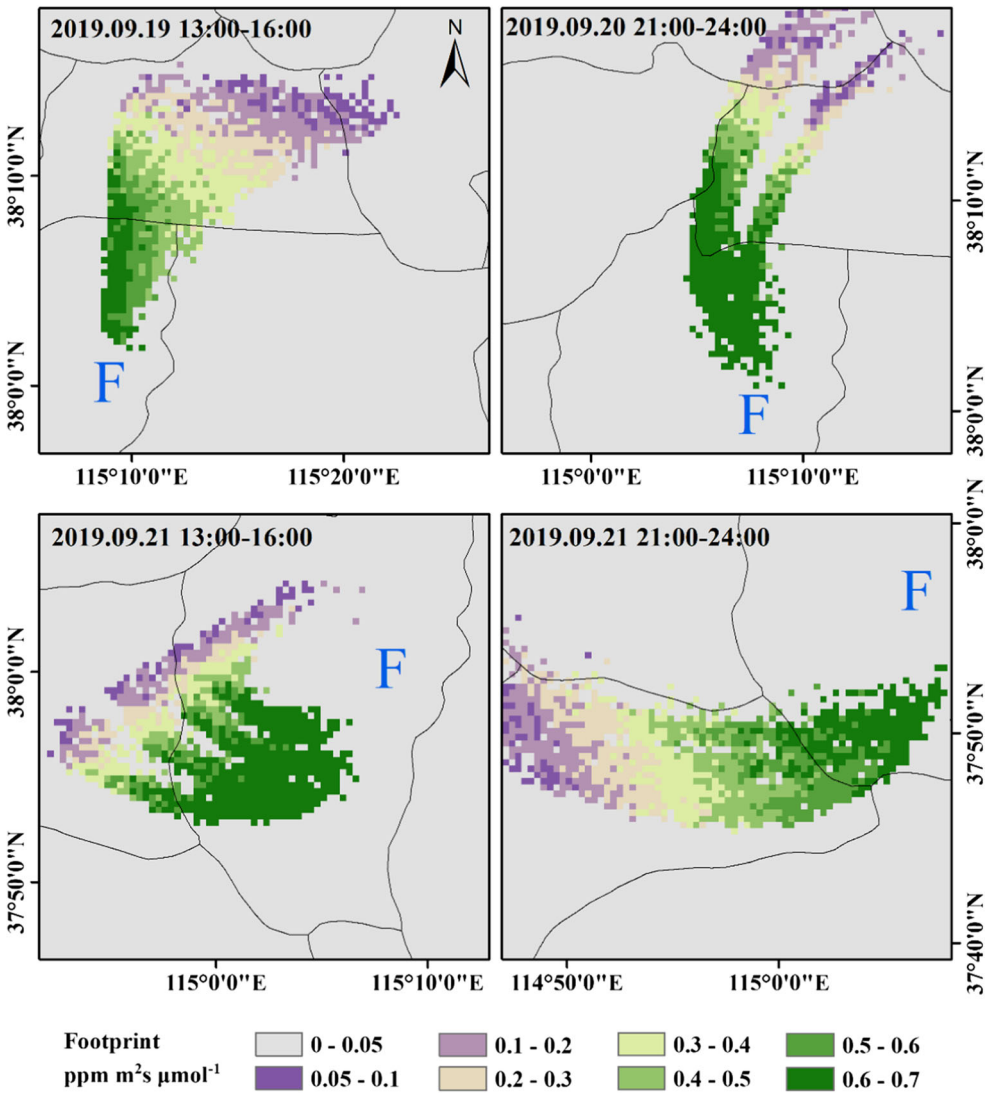

Fig. 6 Distribution map of the forward trajectory near the study area simulated by WRF-STILT. "F" denotes the factory

quality of surrounding regions. For example, we found that the transport direction of the air pollutants from the factory examined was mainly towards urban areas of Xinji during the study period, implying that the emissions from this factory are not conducive to the pollution control of the city in autumn.

Conclusions

This study investigates the transport and impacts of air pollutants from a fixed location factory emission, by using both the mobile observations and WRF-STILT model simulations. Both observation and model analyses show significant impacts from the factory emissions on the surrounding regions within 3 km away from it, and show that the influence from the factory emissions increases first and then decreases with the distance before stabilizing around a low value.

The mobile observations from September 19 to September 21, 2019, shows that the concentrations of $PM_{2.5}$, SO_2, and NO_2 have peak values at a distance around 0.5–3 km from the emission source, and the peak value of $PM_{2.5}$ appears much closer to the emission source than that of SO_2 and NO_2. Further quantification analysis shows that the factory emission has a higher contribution rate to the air pollution within 3 km around the emission source, and the contribution rate at night (10–48%) is significantly higher than that during daytime (3–23%). WRF-STILT model simulation analysis also shows that with the distance from the emission source increasing, the pollution concentrations gradually decrease and the meteorological conditions are an important factor driving the diffusion of pollutants. The results shown in this study suggests that effective air quality control strategy should consider sufficiently the direction and influential distance of pollutants from emission sources, and establish the relationship between emissions from a given source and near surface air quality of surrounding regions.

Supplementary Information The online version contains supplementary material available at https://doi.org/10.1007/s11869-021-01023-9.

Funding This research was funded by the Beijing Municipal Commission of Science and Technology (grant D171100007917001), the National Natural Science Foundation of China (grant 41925022), and the State Key Laboratory of Earth Surface Processes and Resource Ecology.

Data availability The data is available by request to Hao Fan via fanhao_geo@163.com.

References

An ZS, Huang RJ, Zhang RY, Tie XX, Li GH, Cao JJ, Zhou WJ, Shi ZG, Han YM, Gu ZL, Ji YM (2019) Severe haze in northern China: a synergy of anthropogenic emissions and atmospheric processes. Proc Natl Acad Sci U S A 116(18):8657–8666. https://doi.org/10.1073/pnas.1900125116

Brophy K, Graven H, Manning AJ, White E, Arnold T, Fischer ML, Jeong S, Cui X, Rigby M (2019) Characterizing uncertainties in atmospheric inversions of fossil fuel CO_2 emissions in California. Atmos Chem Phys 19(5):2991–3006. https://doi.org/10.5194/acp-19-2991-2019

Chen Z, Chen D, Wen W, Zhuang Y, Kwan M-P, Chen B, Zhao B, Yang L, Gao B, Li R, Xu B (2019) Evaluating the "2+26" regional strategy for air quality improvement during two air pollution alerts in Beijing: variations in $PM_{2.5}$ concentrations, source apportionment, and the relative contribution of local emission and regional transport. Atmos Chem Phys 19:6879–6891. https://doi.org/10.5194/acp-19-6879-2019

Cheng X, Ma J, Jin J, Guo J, Liu Y, Peng J, Ma X, Qian M, Xia Q, Yan P (2020) Retrieving tropospheric NO_2 vertical column densities around the city of Beijing and estimating NOx emissions based on car MAX-DOAS measurements. Atmos Chem Phys 20:10757–10774. https://doi.org/10.5194/acp-20-10757-2020

Cohen AJ, Brauer M, Burnett R, Anderson HR, Frostad J, Estep K, Balakrishnan K, Brunekreef B, Dandona L, Dandona R, Feigin V, Freedman G, Hubbell B, Jobling A, Kan H, Knibbs L, Liu Y, Martin R, Morawska L, Pope CA, Shin H, Straif K, Shaddick G, Thomas M, van Dingenen R, van Donkelaar A, Vos T, Murray CJL, Forouzanfar MH (2017) Estimates and 25-year trends of the global burden of disease attributable to ambient air pollution: an analysis of data from the global burden of diseases study 2015. Lancet. 389:1907–1918. https://doi.org/10.1016/S0140-6736(17)30505-6

Dang R, Liao H (2019) Severe winter haze days in the Beijing–Tianjin–Hebei region from 1985 to 2017 and the roles of anthropogenic emissions and meteorology. Atmos Chem Phys 19:10801–10816. https://doi.org/10.5194/acp-19-10801-2019

Ding JY, Miyazaki K, van der A RJ, Mijling B, Kurokawa J-I, Cho SY, Janssens-Maenhout G, Zhang Q, Liu F, Levelt PF (2017) Intercomparison of NOx emission inventories over East Asia. Atmos Chem Phys 17(16):10125–10141. https://doi.org/10.5194/acp-17-10125-2017

Doherty RM, Orbe C, Zeng G, Plummer DA, Prather MJ, Wild O, Lin M, Shindell DT, Mackenzie IA (2017) Multi-model impacts of climate change on pollution transport from global emission source regions. Atmos Chem Phys 17:14219–14237. https://doi.org/10.5194/acp-17-14219-2017

Fan H, Zhao C, Yang Y (2020a) A comprehensive analysis about the spatio-temporal variation of urban air pollution in China during recent years of 2014-2018. Atmos Environ 220:117066. https://doi.org/10.1016/j.atmosenv.2019.117066

Fan H, Zhao CF, Ma ZS, Yang YK (2020b) Atmospheric inverse estimates of CO emissions from Zhengzhou, China. Environ Pollut 267:115164. https://doi.org/10.1016/j.envpol.2020.115164

Feng J, Chan E, Vet R (2020) Air quality in the eastern United States and Eastern Canada for 1990–2015: 25 years of change in response to emission reductions of SO_2 and NOx in the region. Atmos Chem Phys 20:3107–3134. https://doi.org/10.5194/acp-20-3107-2020

Fischer H, Pozzer A, Schmitt T, Jöckel P, Klippel T, Taraborrelli D, Lelieveld J (2015) Hydrogen peroxide in the marine boundary layer over the South Atlantic during the OOMPH cruise in March 2007. Atmos Chem Phys 15:6971–6980. https://doi.org/10.5194/acp-15-6971-2015

Georgiou GK, Christoudias T, Proestos Y, Kushta J, Hadjinicolaou P, Lelieveld J (2018) Air quality modelling in the summer over the eastern Mediterranean using WRF-Chem: chemistry and aerosol mechanism intercomparison. Atmos Chem Phys 18:1555–1571. https://doi.org/10.5194/acp-18-1555-2018

Heintzenberg J, Birmili W, Hellack B, Spindler G, Tuch T, Wiedensohler A (2020) Aerosol pollution maps and trends over Germany with hourly data at four rural background stations from 2009 to 2018. Atmos Chem Phys 20:10967–10984. https://doi.org/10.5194/acp-20-10967-2020

Hilario MRA, Cruz MT, Cambaliza MOL, Reid JS, Xian P, Simpas JB, Lagrosas ND, Uy SNY, Cliff S, Zhao Y (2020) Investigating size-segregated sources of elemental composition of particulate matter in the South China Sea during the 2011 Vasco cruise. Atmos Chem Phys 20:1255–1276. https://doi.org/10.5194/acp-20-1255-2020

Hu J, Li X, Huang L, Ying Q, Zhang Q, Zhao B, Wang S, Zhang H (2017) Ensemble prediction of air quality using the WRF/CMAQ model system for health effect studies in China. Atmos Chem Phys 17:13103–13118. https://doi.org/10.5194/acp-17-13103-2017

Hu C, Griffis TJ, Lee X, Millet DB, Chen Z, Baker JM, Xiao K (2018) Top-down constraints on anthropogenic CO_2 emissions within an agricultural-urban landscape. J Geophys Res Atmos 123(9):4674–4694. https://doi.org/10.1029/2017jd027881

Huang R-J, Wang Y, Cao J, Lin C, Duan J, Chen Q, Li Y, Gu Y, Yan J, Xu W, Fröhlich R, Canonaco F, Bozzetti C, Ovadnevaite J, Ceburnis D, Canagaratna MR, Jayne J, Worsnop DR, El-Haddad I, Prévôt ASH, O'Dowd CD (2019) Primary emissions versus secondary formation of fine particulate matter in the most polluted city (Shijiazhuang) in North China. Atmos Chem Phys 19:2283–2298. https://doi.org/10.5194/acp-19-2283-2019

Jeong S, Zhao CF, Andrews AE, Dlugokencky EJ, Sweeney C, Bianco L, Wilczak JM, Fischer ML (2012a) Seasonal variations in N_2O emissions from central California. Geophys Res Lett 39(16). https://doi.org/10.1029/2012gl052307

Jeong S, Zhao CF, Andrews AE, Bianco L, Wilczak JM, Fischer ML (2012b) Seasonal variation of CH_4 emissions from central California. J Geophys Res Atmos 117:D11306. https://doi.org/10.1029/2011JD016896

Kontkanen J, Deng C, Fu Y, Dada L, Zhou Y, Cai J, Daellenbach KR, Hakala S, Kokkonen TV, Lin Z, Liu Y, Wang Y, Yan C, Petäjä T, Jiang J, Kulmala M, Paasonen P (2020) Size-resolved particle number emissions in Beijing determined from measured particle size distributions. Atmos Chem Phys 20:11329–11348. https://doi.org/10.5194/acp-20-11329-2020

Kuik F, Kerschbaumer A, Lauer A, Lupascu A, von Schneidemesser E, Butler TM (2018) Top–down quantification of NOx emissions from traffic in an urban area using a high-resolution regional atmospheric chemistry model. Atmos Chem Phys 18:8203–8225. https://doi.org/10.5194/acp-18-8203-2018

Lachatre M, Fortems-Cheiney A, Foret G, Siour G, Dufour G, Clarisse L, Clerbaux C, Coheur P-F, Van Damme M, Beekmann M (2019) The unintended consequence of SO_2 and NO_2 regulations over China: increase of ammonia levels and impact on $PM_{2.5}$ concentrations. Atmos Chem Phys 19:6701–6716. https://doi.org/10.5194/acp-19-6701-2019

Li Z, Lau WK-M, Ramanathan V, Wu G, Ding Y, Manoj MG, Liu J, Qian Y, Li J, Zhou T, Fan J, Rosenfeld D, Ming Y, Wang Y, Huang J, Wang B, Xu X, Lee S-S, Cribb M, Zhang F, Yang X, Zhao C, Takemura T, Wang K, Xia X, Yin Y, Zhang H, Guo J, Zhai PM, Sugimoto N, Babu SS, Brasseur GP (2016) Aerosol and monsoon climate interactions over Asia. Rev Geophys 54:866–929. https://doi.org/10.1002/2015RG000500

Li Z, Li C, Ye X, Fu H, Wang L, Yang X, Wang X, Zhao Z, Kan H, Mellouki A, Chen J (2018) Air quality in the middle and lower reaches of the Yangtze River channel: a cruise campaign. Atmos Chem Phys 18:14445–14464. https://doi.org/10.5194/acp-18-14445-2018

Li K, Jacob DJ, Liao H, Shen L, Zhang Q, Bates KH (2019) Anthropogenic drivers of 2013–2017 trends in summer surface ozone in China. Proc Natl Acad Sci USA 116(2):422–427. https://doi.org/10.1073/pnas.1812168116

Li J, Han Z, Wu Y, Xiong Z, Xia X, Li J, Liang L, Zhang R (2020) Aerosol radiative effects and feedbacks on boundary layer meteorology and $PM_{2.5}$ chemical components during winter haze events over the Beijing-Tianjin-Hebei region. Atmos Chem Phys 20:8659–8690. https://doi.org/10.5194/acp-20-8659-2020

Lin JC, Gerbig C, Wofsy SC, Andrews AE, Daube BC, Davis KJ (2003) A nearfield tool for simulating the upstream influence of atmospheric observations: the Stochastic Time-Inverted Lagrangian Transport (STILT) model. J Geophys Res Atmos 108(D16). https://doi.org/10.1029/2002jd003161

Lugon L, Sartelet K, Kim Y, Vigneron J, Chrétien O (2020) Nonstationary modeling of NO_2, NO and NOx in Paris using the Street-in-Grid model: coupling local and regional scales with a two-way dynamic approach. Atmos Chem Phys 20:7717–7740. https://doi.org/10.5194/acp-20-7717-2020

Mao JB, Zhang Y, Yu FQ, Chen JM, Sun JF, Wang SS, Zuo Z, Zhou J, Yu Q, Ma WC, Chen LM (2020) Simulating the impacts of ship emissions on coastal air quality: Importance of a high-resolution emission inventory relative to cruise and land-based observations. Sci Total Environ 728:138454. https://doi.org/10.1016/j.scitotenv.2020.138454

Nehrkorn T, Eluszkiewicz J, Wofsy SC, Lin JC, Gerbig C, Longo M, Freitas S (2010) Coupled weather research and forecasting stochastic time-inverted Lagrangian transport (WRF-STILT) model. Meteorog Atmos Phys 107(1-2):51–64. https://doi.org/10.1007/s00703-010-0068-x

Ohara T, Akimoto H, Kurokawa J, Horii N, Yamaji K, Yan X, Hayasaka T (2007) An Asian emission inventory of anthropogenic emission sources for the period 1980–2020. Atmos Chem Phys 7:4419–4444

Sahu SK, Chen L, Liu S, Ding D, Xing J (2020) The impact of aerosol direct radiative effects on $PM_{2.5}$-related health risk in northern hemisphere during 2013–2017. Chemosphere. 254:126832–126840. https://doi.org/10.1016/j.chemosphere.2020.126832

Shi X, Zhao C, Jiang JH, Wang C, Yang X, Yung YL (2018) Spatial representativeness of $PM_{2.5}$ concentrations obtained using observations from network stations. J Geophys Res Atmos 123:3145–3158. https://doi.org/10.1002/2017JD027913

Vandyck T, Keramidas K, Kitous A, Spadaro JV, Van Dingenen R, Holland M, Saveyn B (2018) Air quality co-benefits for human health and agriculture counterbalance costs to meet Paris Agreement pledges. Nat Commun 9(1):4939. https://doi.org/10.1038/s41467-018-06885-9

Wang Q, Liu S, Li N, Dai W, Wu Y, Tian J, Zhou Y, Wang M, Ho SSH, Chen Y, Zhang R, Zhao S, Zhu C, Han Y, Tie X, Cao J (2019) Impacts of short-term mitigation measures on $PM_{2.5}$ and radiative effects: a case study at a regional background site near Beijing, China. Atmos Chem Phys 19:1881–1899. https://doi.org/10.5194/acp-19-1881-2019

Yang X, Zhao C, Guo J, Wang Y (2016) Intensification of aerosol pollution associated with its feedback with surface solar radiation and winds in Beijing. J Geophys Res Atmos 121:4093–4099. https://doi.org/10.1002/2015JD024645

Zhai S, An X, Zhao T, Sun Z, Wang W, Hou Q, Guo Z, Wang C (2018) Detection of critical $PM_{2.5}$ emission sources and their contributions to a heavy haze episode in Beijing, China, using an adjoint model. Atmos Chem Phys 18:6241–6258. https://doi.org/10.5194/acp-18-6241-2018

Zhang Q, Zheng YX, Tong D, Shao M, Wang SX, Zhang YH, Xu XD, Wang JN, He H, Liu WQ, Ding YH, Lei Y, Li JH, Wang ZF, Zhang XY, Wang YS, Cheng J, Liu Y, Shi QR, Yan L, Geng GN, Hong

CP, Li M, Liu F, Zheng B, Cao JJ, Ding AJ, Gao J, Fu QY, Huo JT, Liu BX, Liu ZR, Yang FM, He KB, Hao JM (2019) Drivers of improved $PM_{2.5}$ air quality in China from 2013 to 2017. Proc Natl Acad Sci USA 116(49):24463–24469. https://doi.org/10.1073/pnas.1907956116

Zhao CF, Andrews AE, Bianco L, Eluszkiewicz J, Hirsch A, MacDonald C, Nehrkorn T, Fischer ML (2009) Atmospheric inverse estimates of methane emissions from Central California. J Geophys Res Atmos 114:D16302. https://doi.org/10.1029/2008jd011671

Zhao CF, Lin YL, Wu F, Wang Y, Li ZQ, Rosenfeld D, Wang Y (2018) Enlarging rainfall area of tropical cyclones by atmospheric aerosols. Geophys Res Lett 45(16):8604–8611. https://doi.org/10.1029/2018GL079427

Zhao CF, Wang Y, Shi XQ, Zhang DZ, Wang CY, Jiang JH, Zhang Q, Fan H (2019) Estimating the contribution of local primary emissions to particulate pollution using high-density station observations. J Geophys Res Atmos 124(3):1648–1661. https://doi.org/10.1029/2018jd028888

Zhao CF, Yang YK, Fan H, Huang JP, Fu YF, Zhang XY, Kang SC, Cong ZY, Letu H, Menenti M (2020) Aerosol characteristics and impacts on weather and climate over Tibetan Plateau. Natl Sci Rev 7(3):492–495. https://doi.org/10.1093/nsr/nwz184.nwz184